Confinement Enhances the Diversity of Microbial Flow Fields

Raphaël Jeanneret,[1,3] Dmitri O. Pushkin,[2] and Marco Polin[3,4,*]
[1]IMEDEA, University of the Balearic Islands, Carrer de Miquel Marquès, 21, 07190 Esporles, Spain
[2]Mathematics Department, University of York, Heslington, York, YO10 5DD, United Kingdom
[3]Department of Physics, University of Warwick, Gibbet Hill Road, Coventry CV4 7AL, United Kingdom
[4]Centre For Mechanochemical Cell Biology, University of Warwick, Gibbet Hill Road, Coventry CV4 7AL, United Kingdom

(Received 17 April 2019; revised manuscript received 22 July 2019; published 13 December 2019)

Despite their importance in many biological, ecological, and physical processes, microorganismal fluid flows under tight confinement have not been investigated experimentally. Strong screening of Stokelets in this geometry suggests that the flow fields of different microorganisms should be universally dominated by the 2D source dipole from the swimmer's finite-size body. Confinement therefore is poised to collapse differences across microorganisms, which are instead well established in bulk. We combine experiments and theoretical modeling to show that, in general, this is not correct. Our results demonstrate that potentially minute details like microswimmer spinning and the physical arrangement of the propulsion appendages have in fact a leading role in setting qualitative topological properties of the hydrodynamic flow fields of microswimmers under confinement. This is well captured by an effective 2D model, even under relatively weak confinement. These results imply that active confined hydrodynamics is much richer than in bulk and depends in a subtle manner on the size, shape, and propulsion mechanisms of the active components.

DOI: 10.1103/PhysRevLett.123.248102

The way fluid is displaced around microswimmers is crucial to many biological, ecological, and physical processes [1]. For instance, the uptake of nutrients and capture of small prey by microorganisms depends directly on their flow fields [2–7], planktonic predators and prey detect each other mostly via fluid-mediated mechanosensing [8–12], and some species of protists can even relay information on potential nearby danger via hydrodynamic trigger waves [13]. The emergence of large-scale collective motion in microswimmer suspensions is also set by the far-field symmetry of the fluid flows from individual active entities [14,15]. Microscopic fluid disturbances naturally fall into the inertialess regime (low Reynolds number), and they are governed by the Stokes equations. In this regime, flows can be decomposed and expanded in terms of singularity solutions, or multipoles [16]. In unbounded fluids, the almost neutrally buoyant swimming microorganisms are generally modeled either as basic force dipoles (stresslets), or with spatially extended dipole variants like the three-forces model introduced for the microalga *Chlamydomonas reinhardtii* (CR) [17] [see Fig. 1(a)]. The resultant flow fields decay as $\sim r^{-2}$ [17,18], and the sign of the effective force dipole divides microswimmers into two large classes: pushers (e.g., bacteria, pushing fluid with their rear-mounted flagella) and pullers (e.g., CR, pulling the fluid with front-mounted cilia). This division appears to be very important in setting macroscopic properties of active fluids, from flow instabilities to bulk rheology [1,19,20]. Biological and artificial active particles, however, are often confined within boundaries, as a consequence of their natural habitat [21–24] or for technological purposes [25] or simply to facilitate experiments [26,27]. In this context, theory has predicted that the bulk flow picture should be critically modified by the boundaries [28,29]. Here we provide a systematic experimental test of these confinement-induced changes in microbial flows.

Important differences are expected in the multipolar expansions of flows from microorganisms between the bulk and confined cases. A point force confined between two parallel no-slip walls creates, in the far field, a fluid disturbance akin to a 2D source dipole with a velocity decay $\sim r^{-2}$ [30]. As noted in [28,29], a force dipole between two plates should then produce a far-field flow decaying as $\sim r^{-3}$, much faster than in bulk. At the same time, whether driven by flows, sedimenting, or self-propelled, a *finite-size* particle moving at a velocity different from the background fluid must induce a source-dipole perturbation along the direction of motion to fulfill mass conservation. In a quasi-2D Hele-Shaw configuration, when the swimmer's size d is comparable to the confinement length H, this singularity decays as $\sim r^{-2}$ [28,31–34] and should therefore dominate the multipolar expansion regardless of the arrangement of propulsive and drag forces. Consequently, confinement should substitute the bulk division between pushers and pullers with a single class of microswimmers whose far-field hydrodynamic interactions are universally mediated by 2D source dipoles, although numerical studies suggest that very near-field details might also be important [29]. These predictions stand in stark contrast to a fundamental lack of systematic

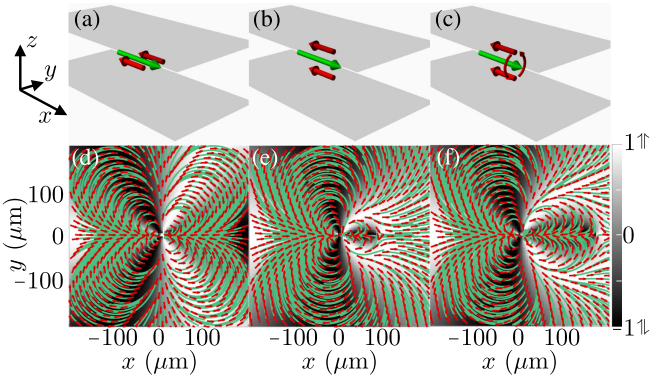

FIG. 1. The far-field signature of a force-free system depends on the relative z position of the forces. Illustrated with a three-forces system. (a),(d) The three forces are in a plane $\parallel$ to the plates. The resulting flow field is quadrupolar with a r^{-3} velocity decay. (b),(e) The forces are in a plane $\perp$ to the plates. The resulting flow field is dipolar with a r^{-2} velocity decay. (c),(f) Effect of spinning the plane of forces. The central quadrupolar region depends on both the radius of the orbit described by the forces and the on-axis separation between thrust and drag (red and green arrows, respectively, in the first row). Gray scale shows $\cos(\alpha)$, where α is the angle between the local velocity and the swimming axis x.

experimental investigations to test and substantiate the theoretical picture (but see Refs. [35,36] for the collective effects in confined active droplets).

In this Letter, we combine systematic experiments with modeling to show that, within the experimentally accessible range, confinement does not lead to a universal collapse of microbial flows. Instead, we observe strong qualitative differences resulting from details in the geometry and propulsion of different microbial species. Intuitively, these can be understood to arise from the dependence of wall-induced screening of forces on the forces' position across the sample cell, with the net result of multiplying the variety of microbial flow fields with respect to the bulk case. Despite their sensitivity to the spatial structure of the microswimmer and the level of confinement, the experimental flow fields can be modeled accurately within a 2D thin-film approximation even under relatively weak confinement.

To clarify the effect of confinement, we begin with a simple example. Liron and Mochon [30] showed that a point force $\mathbf{F}_\parallel = (F_x, F_y, 0)$ located at $(x = 0, y = 0, z = h)$ within a Hele-Shaw cell of thickness H in the z direction generates a far-field flow given by

$$\mathbf{u}_{LM,\parallel}(\mathbf{r}, z) = f(z, h, H)(\mathbb{1}/r^2 - 2\mathbf{rr}/r^4) \cdot \mathbf{F}_\parallel, \quad (1)$$

where $\mathbf{r} = (x, y)$ and $f(z, h, H) = -3H/(2\pi\mu)[z/H - (z/H)^2][h/H - (h/H)^2]$. This field is equivalent to a 2D source dipole whose strength $f(z, h, H)$ depends quadratically on the vertical position h of the Stokeslet, with a maximum in the midplane ($h = H/2$). Ignoring temporarily finite-size effects for real microswimmers, this h dependence immediately implies that the flow field created by a force-free swimmer should be qualitatively very sensitive to the spatial arrangement of forces along the z direction because the relative effect of these forces on the fluid can be very different. To illustrate this point, let us consider the three-Stokeslets model for CR [17], where a single force on the fluid representing the cell-body motion [$\mathbf{F}_\parallel$; Figs. 1(a)–1(c), green arrow] is balanced by a pair of forces representing the two front flagella [$-\mathbf{F}_\parallel/2$; Figs. 1(a)–1(c), red arrows]. When the forces are parallel to the xy plane, the far field indeed has a force-dipole symmetry, with a $\sim r^{-3}$ decay as predicted in Ref. [28] [Figs. 1(a) and 1(d)]. However, when the forces lay on a plane *perpendicular* to the xy plane, the far field has a source-dipole symmetry with a slower $\sim r^{-2}$ decay [Figs. 1(b) and 1(e)]. The size of the force-dipole-like recirculation region close to the front of the swimmer [Fig. 1(e)] depends strongly on both the on-axis distance between thrust and drag forces and the separation between the putative flagellar forces. For a swimmer that spins as it swims, as for CR, the topology of the flow field will then oscillate periodically as a function of the rotation of the flagellar plane [see Movie S1 in the Supplemental Material (SM) [37]], and not just as a function of the phase in the beating cycle [26,38]. In this case, the rotation-averaged flow always retains a source-dipole far-field symmetry [Figs. 1(c) and 1(f)], while the extent of the near-field recirculation depends on the separation between the pair of thrust forces (Fig. S1 in the SM [37]). Overall, these arguments suggest that the effective 2D representation of the far-flow field of a confined force-free microswimmer should be guessed with care, as the induced flow has a strong qualitative dependence on the spatial arrangement of the swimmer's propulsion and drag forces. This sensitivity is in sharp contrast with the equivalent case in bulk. It can be understood intuitively as a result of the h dependence of the function $f(z, h, H)$, which implies that a Stokeslet in the midplane produces a z-averaged far-flow field stronger than the one outside it. This consequence of confinement appears to have been largely overlooked, but it could be put to good use to build artificial active systems with *in situ* tunable hydrodynamic interactions, for instance, by modulating the arrangement or orientation of active particles across the Hele-Shaw cell through the application of external fields. Such systems should display a rich set of collective dynamic phenomena.

With this in mind, we now turn to the experiments, measuring flow fields under controlled confinement for both a pullerlike and a pusherlike swimmer, respectively, CR and the dinoflagellate *Oxyrrhis marina* (OM). These organisms have similarly shaped prolate cell bodies [Table S1, Figs. S2(a) and S2(b) in the SM [37]], with diameters $d_{\mathrm{CR}} \lesssim 10$ μm and $d_{\mathrm{OM}} \lesssim 20$ μm, respectively. The former propels with a characteristic breaststroke beating of its pair

of front-mounted flagella ∼12 μm long; the latter employs a ∼30-μm-long back-mounted flagellum which propagates bending waves [Movies S2 and S3 and Figs. S2(a) and S2 (b) in the SM [37]]. Both species spin as they swim. The microorganisms were grown following Ref. [7], then loaded in microfluidic chambers of uniform thickness H ($14\ \mu\text{m} \leq H \leq 60\ \mu\text{m}$) previously passivated with a 0.5% w/v Pluronic F-127 solution. Tracking of 1 μm polystyrene tracer particles (Polysciences, Warrington, Pennsylvania) in the reference frame centered on the microorganism and oriented along its swimming direction was done through a 20 × NA 0.40 objective (Nikon, Japan) at 50 frames/s. This allowed us to reconstruct the induced flow field averaged over the spinning and beating cycles, and across the 10 μm focal volume centered in the middle of the chamber [17,37]. Figures 2(a)–2(e) show the flow fields for CR at five decreasing chamber thicknesses [experimental (numerical) flow fields are shown in blue (green) throughout]. Under weak confinement [$H = 60, 43\ \mu$m; Figs. 2(a) and 2(b)], the flows present a characteristic pullerlike symmetry, with a stagnation point ∼25 μm in front of the cell. Although both features are typical of bulk flows [17], the bulk solution yields in fact poor quantitative agreement, even for $H = 60\ \mu$m (Fig. S3 of the SM [37]). As the channel thickness decreases further [$H = 29$, 21.5, and 14 μm; Figs. 2(c)–2(e)] the flow field clearly develops the structure of a source dipole. The velocity decays as $\sim r^{-2}$, confirming that this is a two-dimensional source dipole (Fig. S4 in the SM [37]). At the same time, close to the cell, the flow presents some differences from a pure 2D source dipole, with a slight front-back asymmetry and side vortices [Figs. 2(c)–2(e)].

Figures 3(a) and 3(b), however, shows that the flows generated by OM in strong confinement ($H = 21.5$ and 29 μm) are qualitatively different from those observed for CR. Within our experimentally accessible range, corresponding to a ∼30× velocity decay for both species (Figs. S4 and S5 in the SM [37]), OM flows display a front-back asymmetric force-dipole field instead of CR's source dipole. This striking difference in flow structure confirms that confinement does not reduce all microbial flows to a unique type but rather makes them very sensitive to precise details of a swimmer's geometry beyond its finite-size body.

To rationalize the measured flows, it is instructive to start first with a simple superposition of the far-field point force solutions from Liron and Mochon [30]. Fitting the average flows of a spinning three-forces model for CR [Fig. 1(c)] and an off-center two-forces one for OM (Fig. S2 in the SM [37]) to the experimental flow fields in $H = 21.5\ \mu$m reveals clearly that both models lack an extra 2D source dipole (Fig. S6 in the SM [37]). This would naturally arise from the cells' finite-size bodies [28] and suggests turning to a conceptually simpler 2D approach, in the spirit of the general treatment of Hele-Shaw flows [39]. The microorganisms, centered in the field of view and swimming along the positive x direction, are modeled by a set of point forces representing drag [strength F_S, position $(x_0, 0)$] and thrust [CR, two point forces of strength $-F_S/2$ at $(x_1, \pm y_1)$; OM, one point force of strength $-F_S$ at $(x_1, 0)$]. Each force is along the x axis and generates a flow given by the Green's function for the effective 2D Stokes equations [37,39]. For no-slip boundaries, the functional shape of this flow depends on a single length

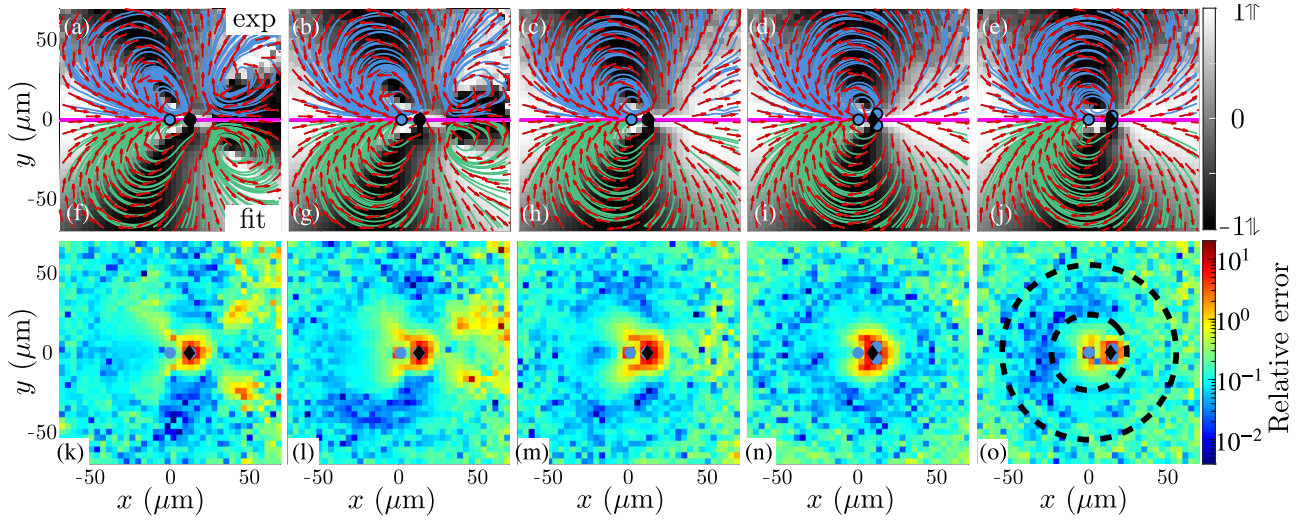

FIG. 2. CR flow fields. (a)–(e) Experimental flow fields for CR for (a) $H = 60\ \mu$m, (b) $H = 43\ \mu$m, (c) $H = 29\ \mu$m, (d) $H = 21.5\ \mu$m, (e) $H = 14\ \mu$m. (f)–(j) Corresponding flow fields obtained from best fits to the effective 2D model. Blue dots, Stokeslet location; black dot, source-dipole location. Gray scale follows the convention in Fig. 1. All panels show streamlines (solid lines) and local velocity vector fields (red arrows). (k)–(o) Magnitudes of the difference between experimental and fitted flows, normalized by the experimental magnitude. Dashed circles in (o) indicate the region of the experimental flows used to determine the best fits.

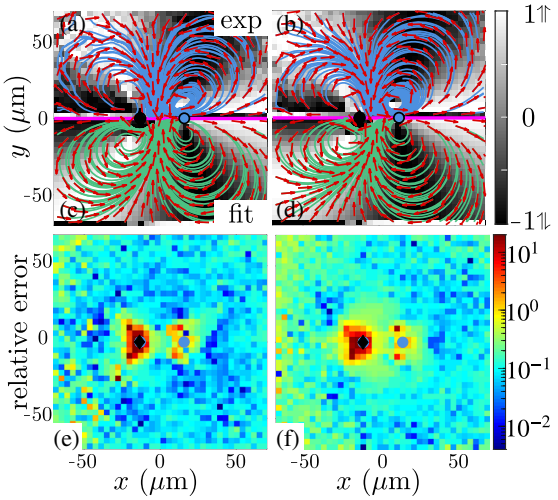

FIG. 3. OM flow fields. Experimental flow fields for OM for (a) $H = 21.5$ μm, (b) $H = 29$ μm. (c),(d) Corresponding flow fields obtained from best fits to the effective 2D model. Blue dots, Stokeslet location; black dot, source-dipole location. Gray scale follows the convention in Fig. 1. All panels show streamlines (solid lines) and local velocity vector fields (red arrows). (e),(f) Magnitudes of the difference between experimental and fitted flows, normalized by the experimental magnitude.

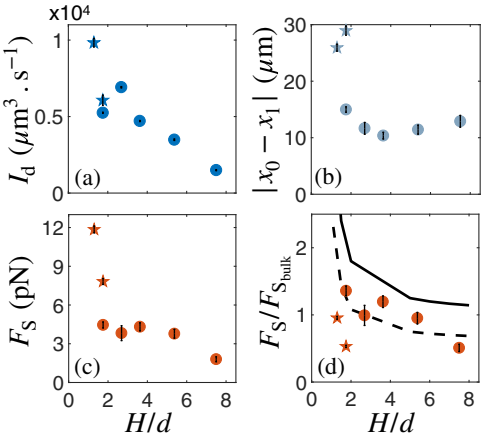

FIG. 4. Dependence of (a) the dipole strength I_d, (b) on-axis force separation $|x_0 - x_1|$, (c) 2D Stokeslet strength F_S as a function of normalized sample thickness H/d for all of the microorganisms studied. OM, ⋆; CR, ∘. (d) F_S normalized by the bulk drag $F_{S_{\text{bulk}}}$ on CM and OM cell bodies modeled as prolate ellipsoids moving at the measured H-dependent speeds. The solid line is the prediction for a sphere of diameter d moving at the center of the Hele-Shaw cell [40]; the dashed line is the solid line diminished by 40%. Error bars throughout represent fit uncertainties to average experimental flow fields.

scale, $\lambda = H/\sqrt{12}$, fixed here by the measured sample thicknesses. The forces are then supplemented by a 2D source dipole $\mathbf{u}_d = -I_d(\mathbf{e}_x/r^2 - 2\mathbf{r}x/r^4)/2\pi$ at position $(x_d, 0)$. It represents both the effect of a finite-size body, and the unequal screening of drag and thrust forces by the walls which is connected to the organism's shape and spinning [see Figs. 1(c) and 1(f)]. The best fits to the experimental data are shown in Figs. 2(f)–2(j) and Figs. 3(c) and 3(d). They were obtained through a systematic sweep in the space of initial parameter values [37] searching for optimal fits to an annular region between 25 and 60 μm around the swimmer [Fig. 2(o), dashed lines]. Within this region, for each one of the 3.7×3.7 μm spatial bins, we collected at least 7×10^3 independent measurements for CR (370 for OM) for each H value (Table S2 in the SM [37]). The fits agree very well with the experiments, with typical relative errors of 15% [Figs. 2(k)–2(o) and Figs. 3(e) and 3(f); Table S3 in the SM [37]]. The model also captures subtle details of the experimental flows. For CR, these include the deformation of the streamlines in front of the organism, the approximate location of the side vortices under strong confinement, and the location of the stagnation point under weak confinement. For OM, the model reproduces the front-back asymmetry of the experimental force-dipole-like field well.

Figure 4 shows the dependence of the main fitting parameters on the reduced sample thickness $H/d_{(\text{CR,OM})}$. The others [CR: (x_d, x_0, y_1); OM: (x_d, x_0)], which encode the spatial structure of the organisms, are consistent across H values (see Fig. S7 in the SM [37]). The error bars represent fit uncertainties to the average experimental flow fields. As expected for weakening confinement, the dipole strength I_d decreases steadily as H/d increases [Fig. 4(a)], along what appears to be a single curve for both microorganisms. The 2D Stokeslet strength F_S, responsible for the thrust, is larger for OM than for CR [$\sim$10 vs 4.2 ± 0.3 pN, respectively; Fig. 4(c)], mirroring differences in size and speed which lead to higher drag for OM than for CR. The values for CR are in line with previous estimates [38] and are largely independent of confinement, although they decrease noticeably for $H = 60$ μm. The fitted propulsive forces F_S can be normalized by the bulk drag for prolate ellipsoids mimicking the swimmers' bodies and translating along the major axis at the measured H-dependent swimming speed. This provides an estimate of the increase in cell-body drag within the Hele-Shaw cells which can be compared with the values predicted for a sphere of radius equal to the cells' semiminor axis [Fig. 4(d), solid line] [37,40]. The latter appears to systematically overestimate the experimental drag estimate by $\sim$40% [Fig. 4(d), dashed line], suggesting that, despite the excellent agreement between the flow fields, F_S might underestimate the full propulsive force of the confined microorganisms. This possibly results from momentum transfer to the surrounding walls in the immediate vicinity of the microorganism. Finally, Fig. 4(b) shows that the fits return an on-axis separation between drag and thrust forces which is both of the correct magnitude and largely independent of the sample thickness H. The large separation for OM is ultimately at the origin of the large asymmetric force-dipole-like flow observed for this organism [Figs. 3(a) and 3(b)]. By artificially reducing

this parameter, the flow acquires a source-dipole structure (Fig. S8 in the SM [37]).

In this Letter, we presented what is, to the best of our knowledge, the first systematic experimental study of the effect of confinement on microswimmer hydrodynamics. In line with previous studies [28,29], the finite-size body and common spinning motion of microorganisms were expected, and observed, to produce a far-field 2D source dipole. However, experiments with OM have highlighted that the spatial structure of a microorganism can easily push this far field to distances where flows are, for practical purposes, negligible. In this case, this leads to strong differences in the topology of OM and CR flows as a result of the on-axis separation between OM's propulsion and drag forces. We expect that these qualitative differences will influence both the biology (e.g., feeding currents) and the physics (e.g., collective behavior) of microorganisms in confinement. Despite qualitative differences, the flows of both microswimmers can be accurately described by considering just a 2D source dipole and a force-free combination of Stokeslets [39]. The latter should reflect the specific arrangement of swimming appendages for each microorganism. We hope that our work will inspire future investigations of the great diversity of fluid flows in confined active matter.

We thank Enkeleida Lushi for the insightful discussions and encouragement. This work was partly supported by a Margalida Comas Fellowship from the Comunitat Autónoma de les Illes Baleares (PD/007/2016) (R. J.).

*M.Polin@warwick.ac.uk

[1] E. Lauga and T. R. Powers, Rep. Prog. Phys. **72**, 096601 (2009).
[2] D. Tam and A. E. Hosoi, Proc. Natl. Acad. Sci. U.S.A. **108**, 1001 (2011).
[3] S. Michelin and E. Lauga, Phys. Fluids **23**, 101901 (2011).
[4] J. Dölger, L. T. Nielsen, T. Kiørboe, and A. Andersen, Sci. Rep. **7**, 39892 (2017).
[5] S. Humphries, Proc. Natl. Acad. Sci. U.S.A. **106**, 7882 (2009).
[6] H. Jashnsaz, M. Al Juboori, C. Weistuch, N. Miller, T. Nguyen, V. Meyerhoff, B. McCoy, S. Perkins, R. Wallgren, B. D. Ray, K. Tsekouras, G. G. Anderson, and S. Pressé, Biophys. J. **112**, 1282 (2017).
[7] A. J. T. M. Mathijssen, R. Jeanneret, and M. Polin, Phys. Rev. Fluids **3**, 033103 (2018).
[8] T. Kiørboe and A. W. Visser, Mar. Ecol. Prog. Ser. **179**, 81 (1999).
[9] H. H. Jakobsen, L. M. Everett, and S. L. Strom, Aquatic Microbial Ecology **44**, 197 (2006).
[10] E. Bruno, C. M. Andersen Borg, and T. Kiørboe, PLoS One **7**, e47906 (2012).
[11] T. Kiørboe, Integr. Comp. Biol. **53**, 821 (2013).
[12] A. Andersen, N. Wadhwa, and T. Kiørboe, Phys. Rev. E **91**, 042712 (2015).
[13] A. J. T. M. Mathijssen, J. Culver, M. S. Bhamla, and M. Prakash, Nature (London) **571**, 560 (2019).
[14] A. Bricard, J.-B. Caussin, N. Desreumaux, O. Dauchot, and D. Bartolo, Nature (London) **503**, 95 (2013).
[15] J. Stenhammar, C. Nardini, R. W. Nash, D. Marenduzzo, and A. Morozov, Phys. Rev. Lett. **119**, 028005 (2017).
[16] K. Sangtae and S. J. Karrila, *Microhydrodynamics: Principles and Selected Applications*, unabridged ed. (Dover Publications, New York, 2005).
[17] K. Drescher, R. E. Goldstein, N. Michel, M. Polin, and I. Tuval, Phys. Rev. Lett. **105**, 168101 (2010).
[18] K. Drescher, J. Dunkel, L. H. Cisneros, S. Ganguly, and R. E. Goldstein, Proc. Natl. Acad. Sci. U.S.A. **108**, 10940 (2011).
[19] S. Rafaï, L. Jibuti, and P. Peyla, Phys. Rev. Lett. **104**, 098102 (2010).
[20] H. M. López, J. Gachelin, C. Douarche, H. Auradou, and E. Clément, Phys. Rev. Lett. **115**, 028301 (2015).
[21] W. Foissner, European Journal of protistology **34**, 195 (1998).
[22] D. Or, B. F. Smets, J. M. Wraith, A. Dechesne, and S. P. Friedman, Adv. Water Resour. **30**, 1505 (2007).
[23] V. Kantsler, J. Dunkel, M. Polin, and R. E. Goldstein, Proc. Natl. Acad. Sci. U.S.A. **110**, 1187 (2013).
[24] J. Elgeti, R. G. Winkler, and G. Gompper, Rep. Prog. Phys. **78**, 056601 (2015).
[25] P. Denissenko, V. Kantsler, D. J. Smith, and J. Kirkman-Brown, Proc. Natl. Acad. Sci. U.S.A. **109**, 8007 (2012).
[26] J. S. Guasto, K. A. Johnson, and J. P. Gollub, Phys. Rev. Lett. **105**, 168102 (2010).
[27] R. E. Pepper, M. Roper, S. Ryu, P. Matsudaira, and H. A. Stone, J. R. Soc. Interface **7**, 851 (2010).
[28] T. Brotto, J.-B. J. Caussin, E. Lauga, and D. Bartolo, Phys. Rev. Lett. **110**, 038101 (2013).
[29] J.-B. Delfau, J. Molina, and M. Sano, Europhys. Lett. **114**, 24001 (2016).
[30] N. Liron and S. Mochon, J. Eng. Math. **10**, 287 (1976).
[31] H. Diamant, J. Phys. Soc. Jpn. **78**, 041002 (2009).
[32] T. Beatus, R. H. Bar-Ziv, and T. Tlusty, Phys. Rep. **516**, 103 (2012).
[33] P. J. Janssen, M. D. Baron, P. D. Anderson, J. Blawzdziewicz, M. Loewenberg, and E. Wajnryb, Soft Matter **8**, 7495 (2012).
[34] N. Desreumaux, J.-B. Caussin, R. Jeanneret, E. Lauga, and D. Bartolo, Phys. Rev. Lett. **111**, 118301 (2013).
[35] C. Krüger, C. Bahr, S. Herminghaus, and C. C. Maass, Eur. Phys. J. E **39**, 64 (2016).
[36] S. Thutupalli, D. Geyer, R. Singh, R. Adhikari, and H. A. Stone, Proc. Natl. Acad. Sci. U.S.A. **115**, 5403 (2018).
[37] See Supplemental Material at http://link.aps.org/supplemental/10.1103/PhysRevLett.123.248102 for further details on experiments, results and fitting procedure.
[38] G. S. Klindt and B. M. Friedrich, Phys. Rev. E **92**, 063019 (2015).
[39] D. O. Pushkin and M. A. Bees, Advances in Experimental Medicine and Biology **915**, 193 (2016).
[40] P. Ganatos, R. Pfeffer, and S. Weinbaum, J. Fluid Mech. **99**, 755 (1980).